Figure S1: Characterization of known angiogenic signals in skin cell types during wound healing

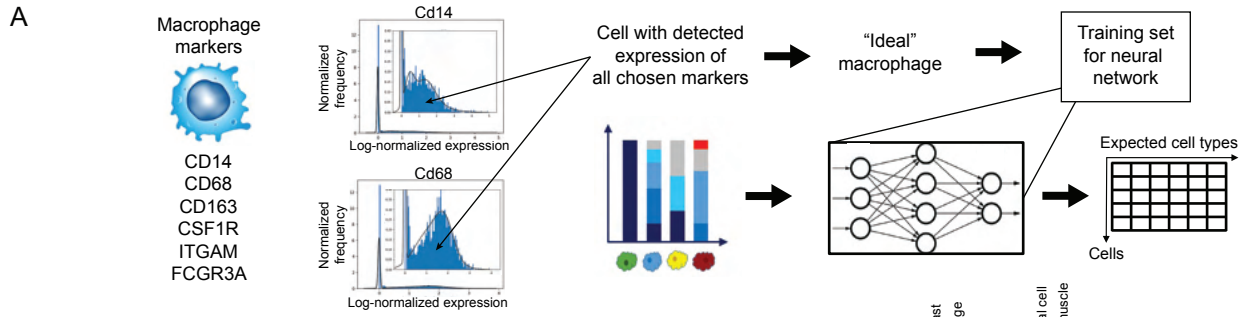

B

CELL TYPE	SELECTED MARKER GENES
Basal	*Krt14, Krt5, Mt2, Krt15, Dnajb1, Fosl1, Fcgbp*
Spinous	*Krt1, Krt10, Krtdap, Mt4, Krt77*
HF/HFSC	*Krt17, Krt79, Cd34*
Fibroblast	*Col1a1, Col1a2, Col3a1, Mfap4, Mfap5, Cpz, Gpx3, Ctsk*
Myofibroblast	*Acta2, Rgs5, Tagln*
Macrophage	*Itgam, Cd14, Cd68, Ccl9, Adgre1 (F4/80)*
Dendritic cell	*Cd74, Cd80, Ccr7, Cd209a*
Langerhans cell	*Cd207, H2-M2, Epcam, Ltc4s*
T cell	*Cd3(d, e, g), Cd28, Cd7, Nkg7, Ctla2a*
Endothelial cell	*Icam1, Icam2, Aqp1, Pecam1*
Skeletal muscle	*Tnnc2, Acta1, Mylpf, Myl1, Tnnt3, Tnni2, Ckm, Pvalb*

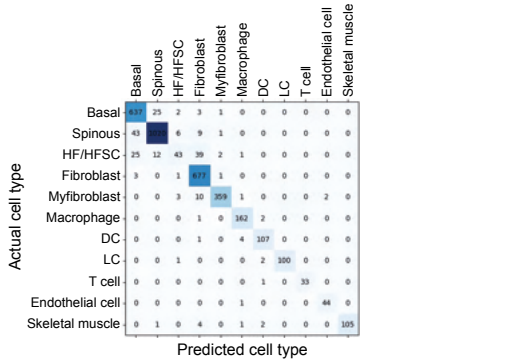

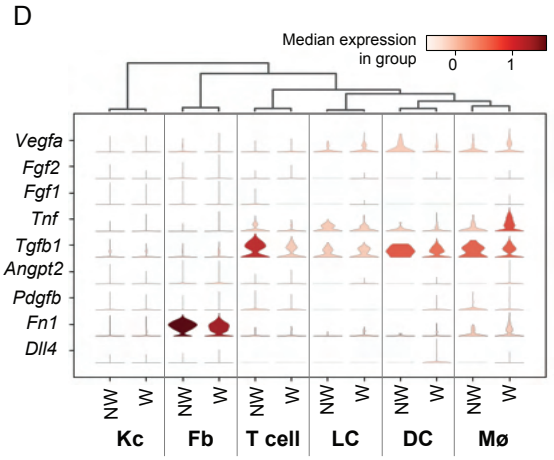

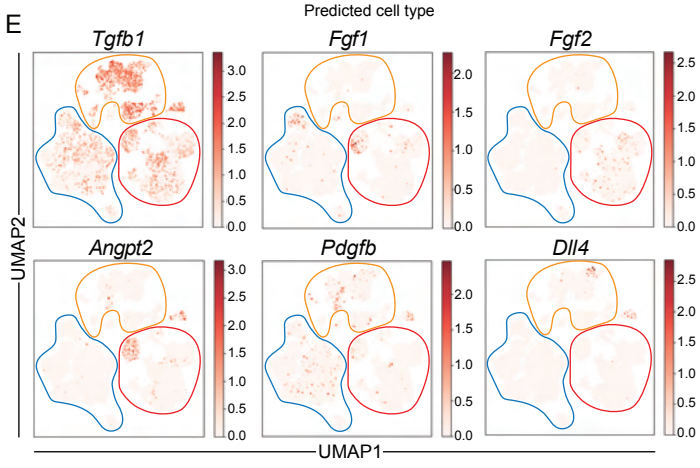

Figure S2: NicheNet predictions of angiogenic signals and ligand-receptor pairs during wound healing

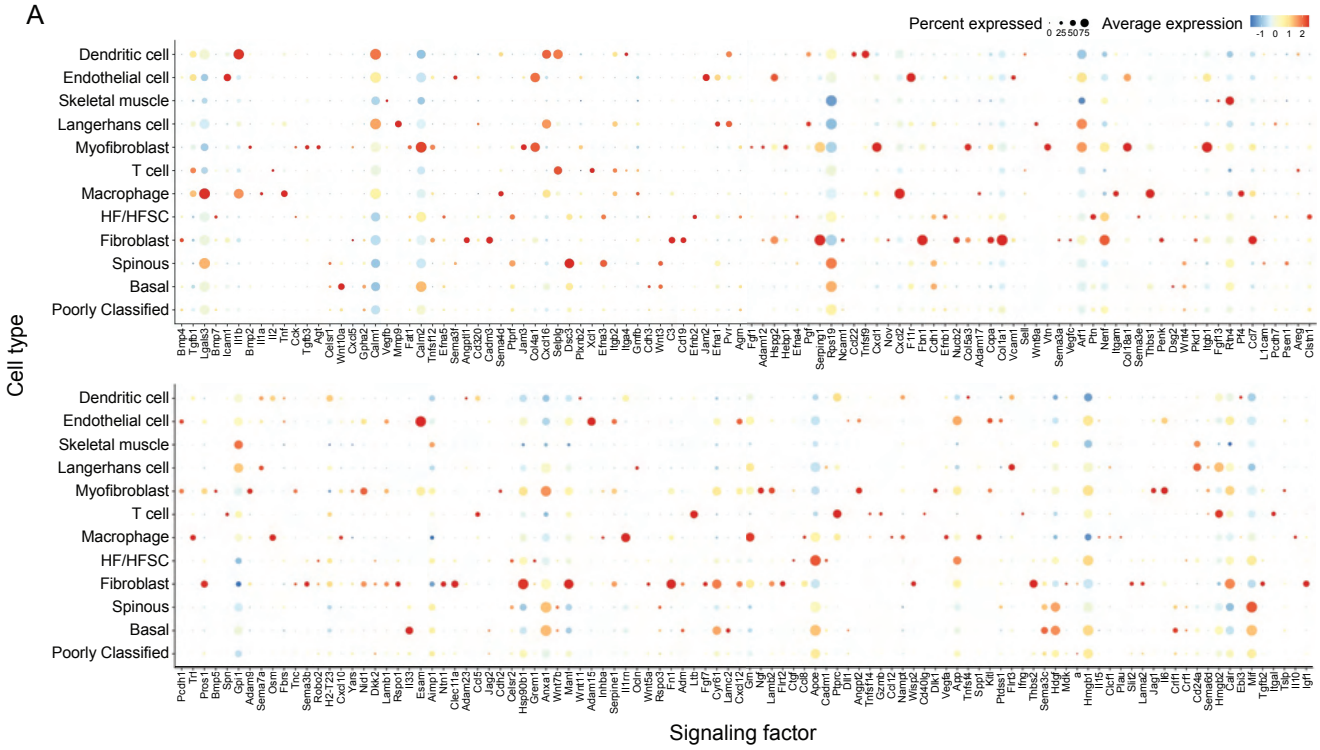

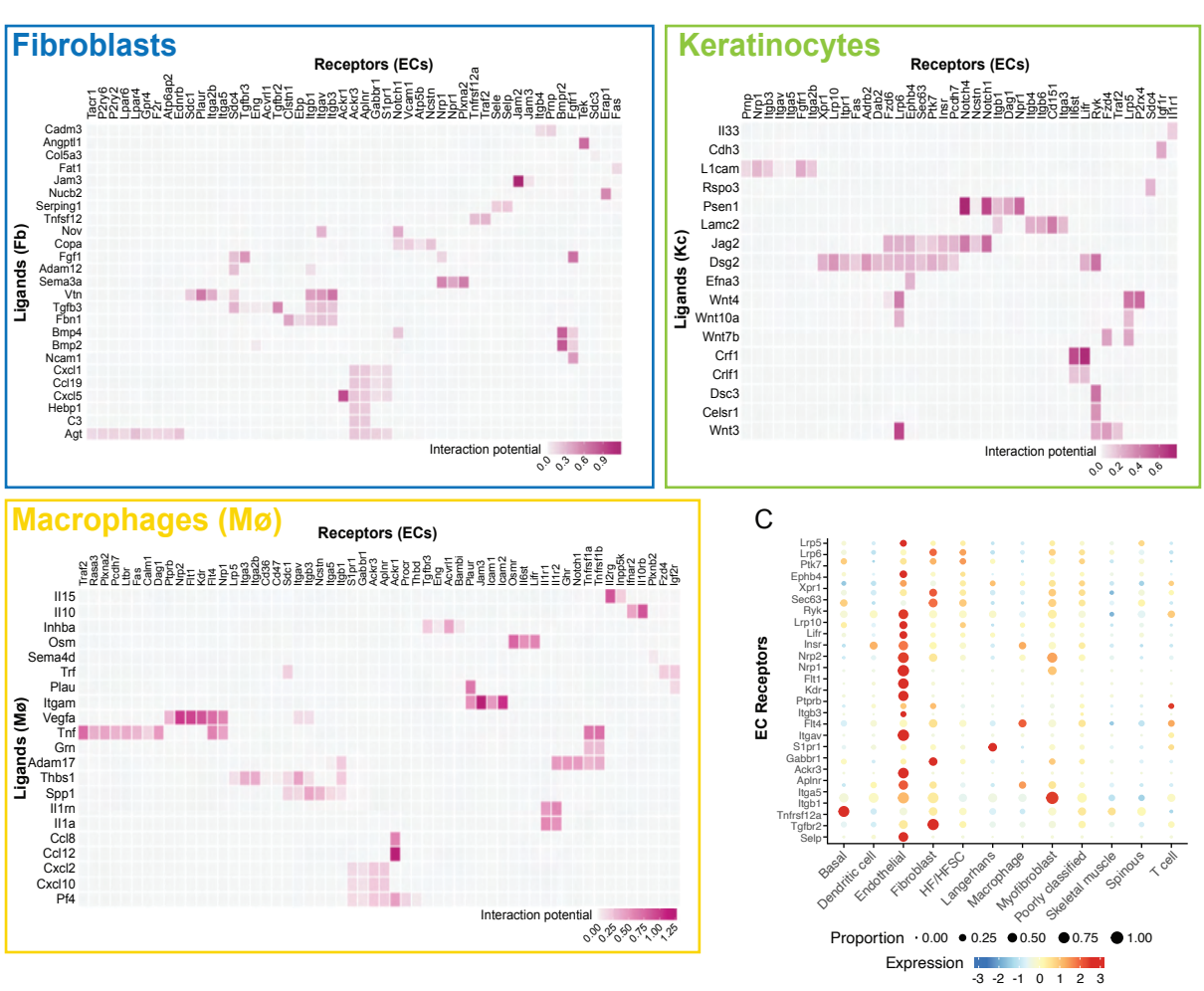

Figure S3: Characterization of Langerhans cell-derived angiogenic factors during skin wound healing

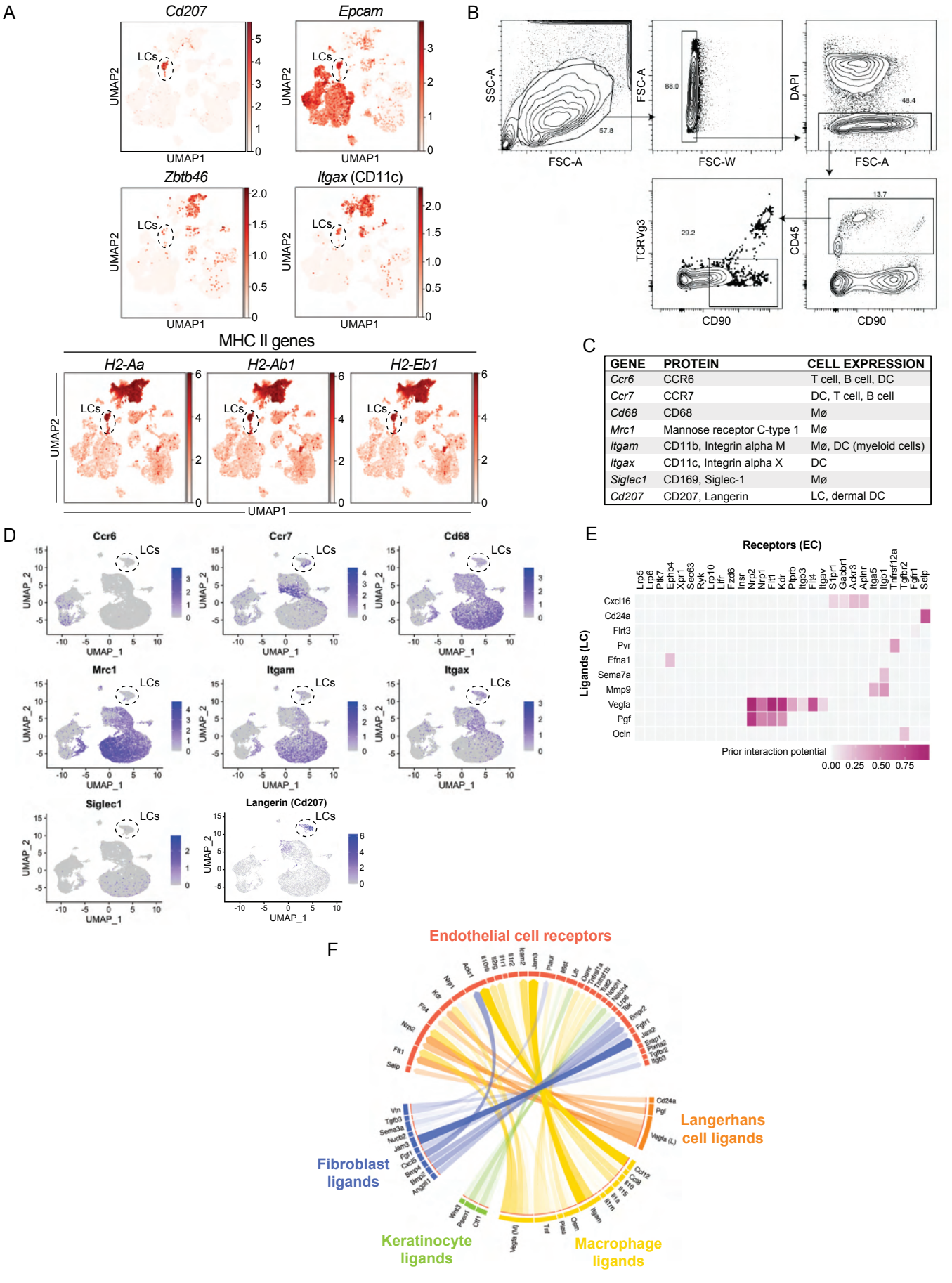

GENE	PROTEIN	CELL EXPRESSION
Ccr6	CCR6	T cell, B cell, DC
Ccr7	CCR7	DC, T cell, B cell
Cd68	CD68	Mø
Mrc1	Mannose receptor C-type 1	Mø
Itgam	CD11b, Integrin alpha M	Mø, DC (myeloid cells)
Itgax	CD11c, Integrin alpha X	DC
Siglec1	CD169, Siglec-1	Mø
Cd207	CD207, Langerin	LC, dermal DC

Figure S4: Langerhans cells are specifically labeled in huLangCreER/mTmG mice.

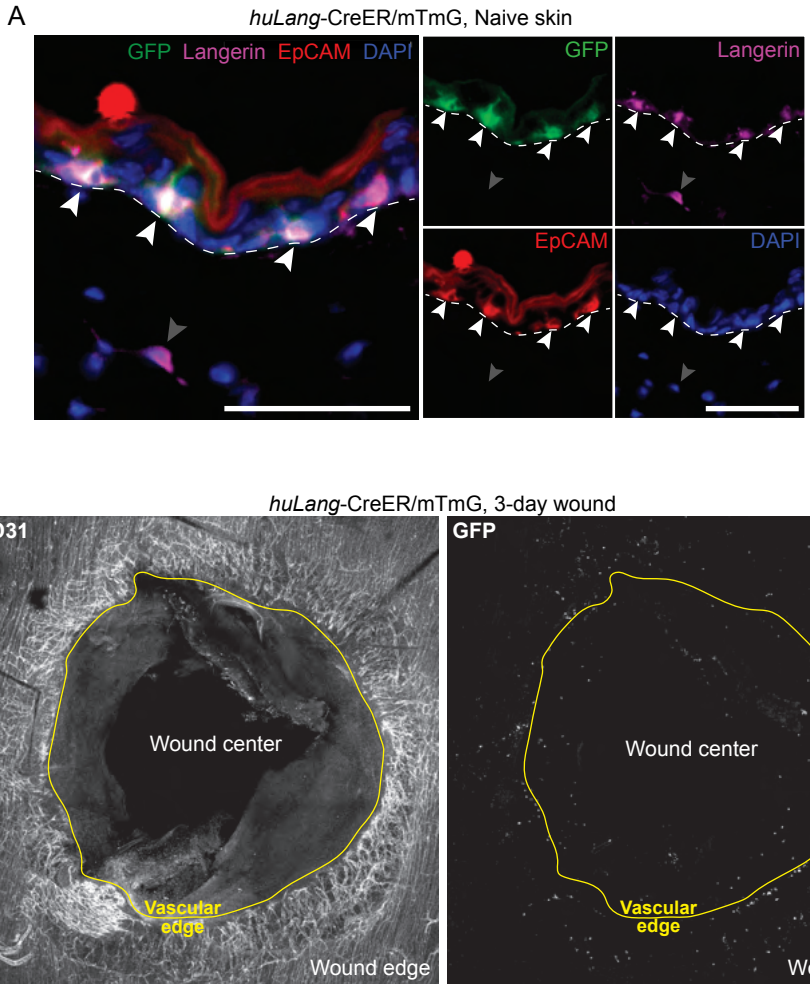

Figure S5 : LC-depleted skin does not have defects in normal morphology nor immune cell recruitment after injury

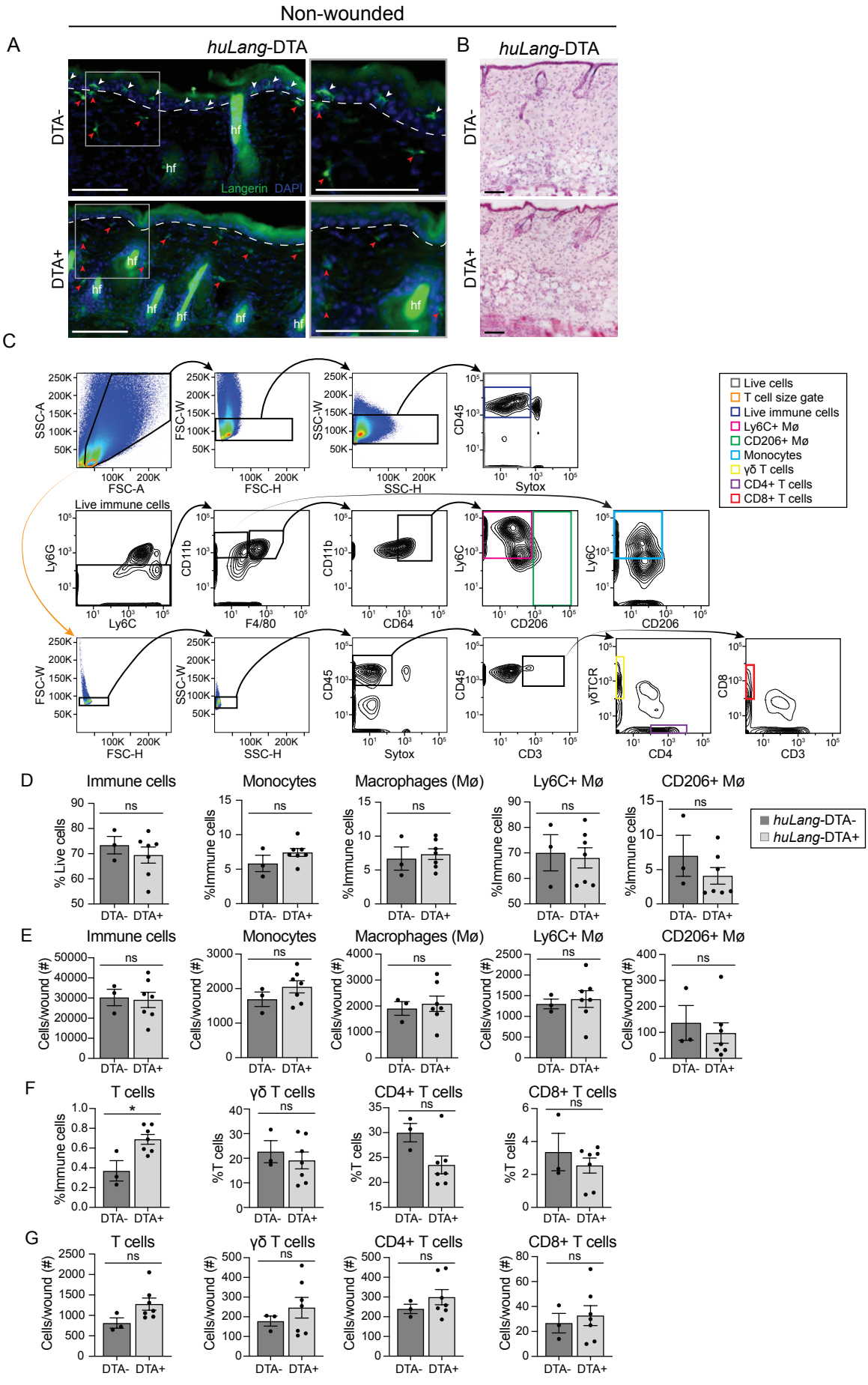

Figure S6: LCs are necessary for efficient wound healing.

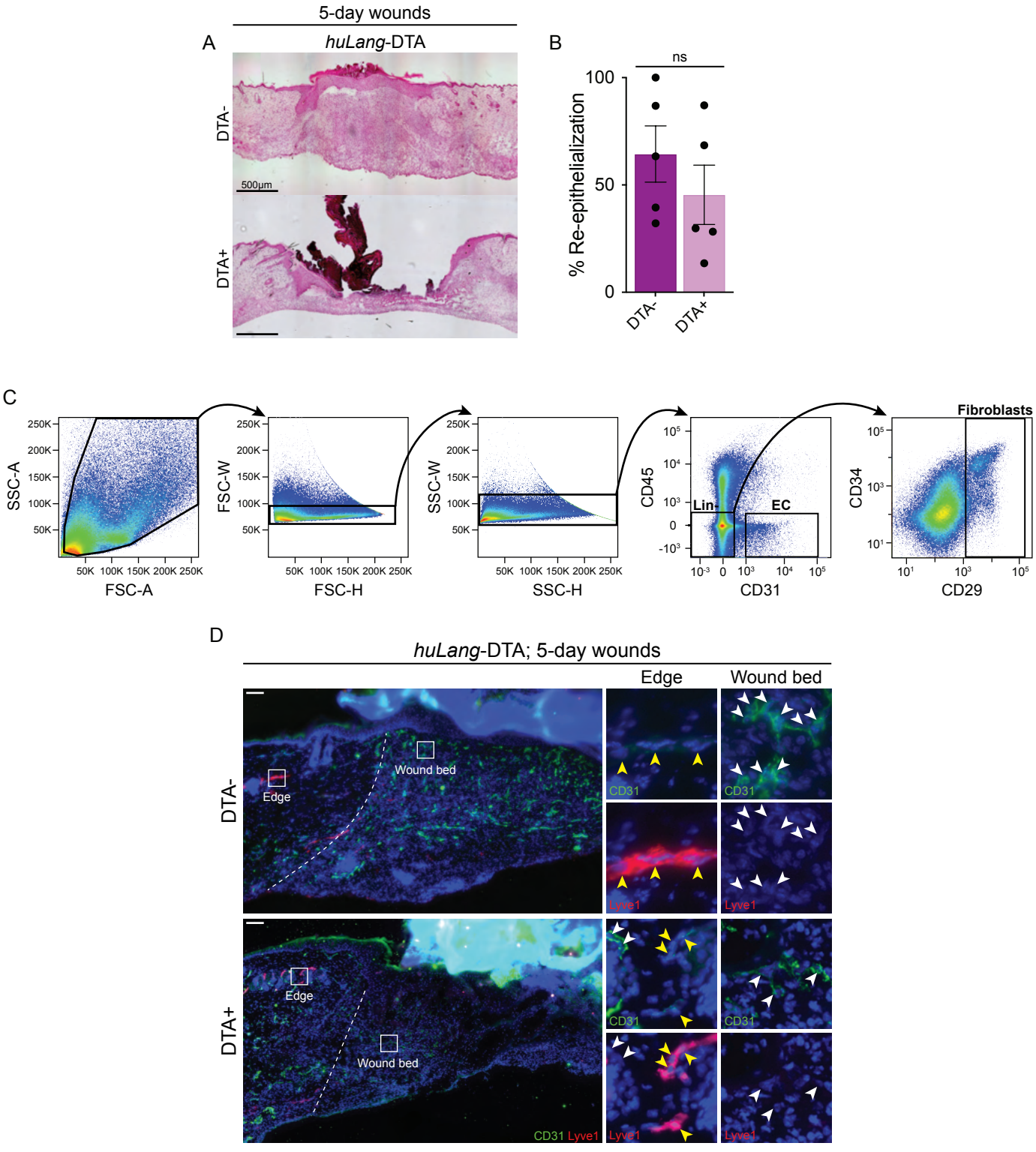

Figure S7: Blood vessel morphology and proliferation is defective in LC-depleted mice

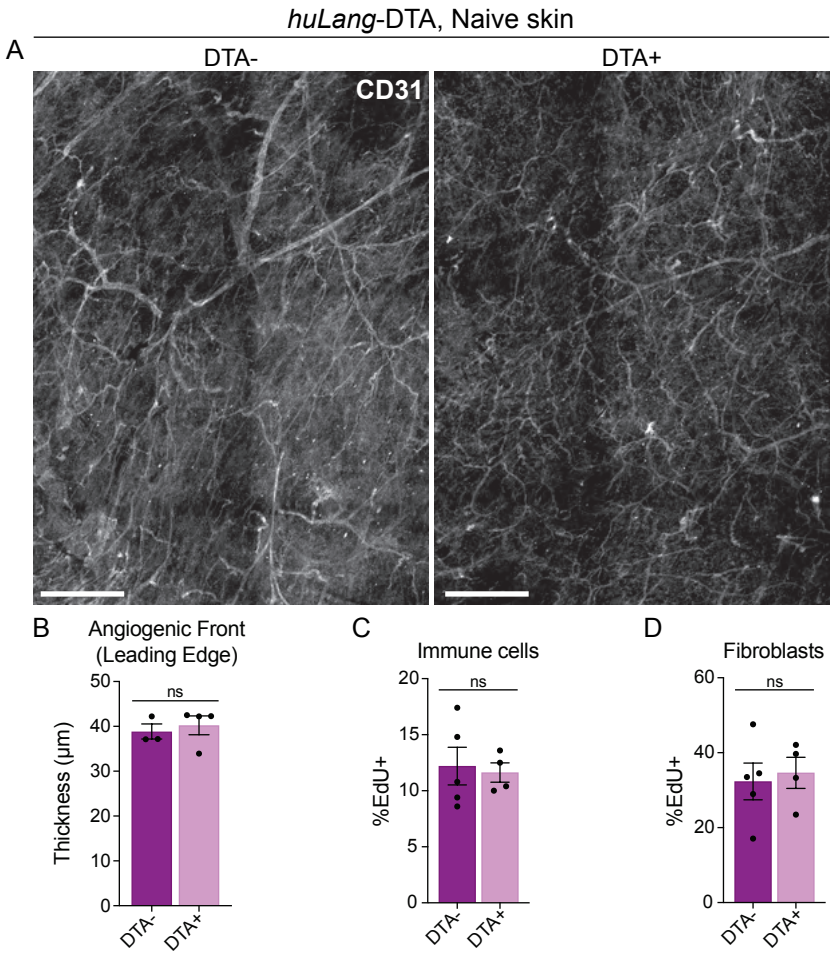

Supplemental figures

Figure S1. Characterization of known angiogenic signals in skin cells during wound healing. Related to Figure 1.

(A) Schematic depicting neural network training for cell type identification, using macrophages as an example. (1) Canonical marker genes for a macrophage are defined, (2) cells with detected expression of all chosen markers are defined as "ideal" macrophages, (3) a training set for the neural network is created [using "ideal" examples of each cell type], (4) neural network scores each cell based on its gene expression and assigns a cell identity.

(B) Table of marker genes defined for each cell type expected in scRNA-seq dataset from purified CD45+ immune cells.

(C) Cell type prediction scores from neural network analysis of GSE142471.

(D) Violin plots depicting median gene expression of established angiogenic genes in keratinocytes (Kc; includes basal, spinous, and HF/HFSC keratinocytes), fibroblasts (Fb; includes myofibroblasts and fibroblasts) T cells, Langerhans cells (LC), dendritic cells (DC), and macrophages (Mø).

(E) Feature plots showing expression of established angiogenic genes (*Tgfb1, Fgf1, Fgf2, Angpt2, Pdgfb,* and *Dll4*) in single cells of Naive and Wounded skin (combined) from Fig. 1B.

Figure S2. NicheNet predictions of angiogenic signals and ligand-receptor pairs during wound healing. Related to Figures 1 and 2.

(A) Bubble plot depicting average mRNA expression (color) of angiogenic signaling factors expressed by different cell types in wounded and nonwounded samples from GSE142471. Signaling factors include the 202 genes identified by NicheNet as potential regulators of the

wound-induced gene expression changes in endothelial cells. Bubble size indicates the percent of cells expressing that gene.

(B) Heatmaps showing potential links between ligands expressed by fibroblasts (Fb), keratinocytes (Kc), and macrophages (Mø) and receptors expressed by endothelial cells (ECs). Fibroblast data includes fibroblast and myofibroblast populations. Keratinocyte data includes basal, spinous, and HF/HFSC populations.

(C) Bubble plot depicting average mRNA expression (color) in each cell population of NicheNet-predicted EC receptors. Bubble size indicates the percent of cells expressing that gene.

Figure S3. Characterization of Langerhans cell-derived angiogenic factors during skin wound healing. Related to Figure 2.

(A) Feature plots depicting expression of canonical LC marker genes: *Cd207, Epcam, Zbtb46, Itgax,* and MHC-II genes (*H2-Aa, H2-Ab1,* and *H2-Eb1*) in scRNA-seq data (GSE142471). Dashed circle highlights the LC population.

(B) FACS sorting scheme to enrich for immune cells for scRNA-seq analysis in GSE166950.

(C) Table depicting immune cell markers and the cell types in which they are expressed.

(D) Feature plots showing expression of established immune cell markers for GSE166950.Dashed circle highlights the LC population.

(E) Heatmaps showing NicheNet-predicted links between ligands expressed by LCs and receptors expressed by endothelial cells (ECs) (GSE142471).

(F) Chord diagram summarizing the top 50 ligand-receptor links during wound healing from GSE142471. Arrows represent ligands from fibroblasts, keratinocytes, macrophages, and Langerhans cells binding to EC receptors.

Figure S4. Langerhans cells are specifically labelled in huLangCreER/mTmG mice. Related to Figure 3.

(A) Fluorescence imaging of GFP+ LCs (green), langerin (magenta), EpCAM (red), and DAPI (blue) in cross-sections of naive skin from LC-iGFP mice. White arrows label GFP+, EpCAM+, langerin+ LCs. Gray arrows label GFP- EpCAM- langerin+ dermal DCs. White dashed line outlines the epidermis. Scale bars, 100 μm.

(B) Maximum intensity projections of confocal imaging of CD31+ blood vessels (left) and GFP+ LCs (right) in 3-day whole mount wounds of LC-iGFP mice. Yellow line outlines the vascular edge of the wound.

Figure S5. LC-depleted skin does not have defects in normal morphology nor immune cell recruitment after injury. Related to Figure 5.

(A) Fluorescence imaging langerin+ LCs and DCs (green) and DAPI (blue) in cross-sections of nonwounded skin from *huLang*-DTA and control mice. White arrows label langerin+ LCs in the epidermis of DTA- samples. Red arrows label langerin+ dDCs in DTA- and DTA+ samples. White dashed lines outline the epidermis. Hair follicles (hf). Scale bars, 100 μm.

(B) Hematoxylin and eosin (H&E) staining of nonwounded skin from *huLang*-DTA+ mice and controls. Scale bars, 100 μm.

(C) Plots depicting the flow cytometry gating strategy to identify and quantify multiple immune cell types: Live cells (Sytox-; gray box), T cell size gate (orange), Live immune cells (CD45+ Sytox-, navy), Ly6C+ macrophages (Mø) (CD45+ Ly6G- CD11b+ F4/80+ CD64+ Ly6C+; pink), CD206+ Mø (CD45+ Ly6G- CD11b+ F4/80+ CD64+ CD206+; green), monocytes (CD45+ Ly6G-

CD11b+ F4/80- Ly6C+; light blue), γδ T cells (CD45+, CD3+, γδTCR+; yellow), CD4 T cells (CD45+, CD3+, CD4+; purple), and CD8 T cells (CD45+, CD3+, CD8+; red).

(D-E) Relative quantification (D) and absolute counts (E) of myeloid cell types (monocytes and macrophages) in 3-day wounds from *huLang*-DTA+ mice and DTA- littermate controls. Data are 3-7 mice. Error bars indicate mean +/- SEM. unpaired T-test, ns, no statistical significance.

(F-G) Relative quantification (F) and absolute counts (G) of T cell populations in 3-day wounds from *huLang*-DTA+ mice and DTA- littermate controls. Data are 3-7 mice. Error bars indicate mean +/- SEM. *$p < 0.05$. ns, no statistical significance.

Figure S6. LCs are necessary for efficient wound healing. Related to Figure 5.

(A) H&E staining of 5-day wounds from *huLang*-DTA+ mice and controls. Scale bars, 500 μm.

(B) Quantification of re-epithelialization as measured by percent of wound bed covered with DAPI+ epithelium in 5-day wounds from *huLang*-DTA+ mice and controls. Data are 5 mice. Error bars indicate mean +/- SEM. unpaired T-test, ns, no statistical significance.

(C) Plots depicting the flow cytometry gating strategy to identify lineage-negative cells (Lin-, CD45- CD31-), endothelial cells (EC, CD31+ CD45-), and fibroblasts (Lin- CD29+).

(D) Representative images of CD31 (green) and Lyve1 (red) immunostaining and DAPI (blue) in cross-sections of 5-day wound beds from *huLang*-DTA and control mice. White arrows indicate CD31+ Lyve1- blood endothelial cells. Yellow arrows indicate $CD31^{-/low}$ Lyve1+ lymphatic endothelial cells. White boxes illustrate the locations of inset images at the wound edge or within the wound bed. White dashed lines delineate wound edges. Scale bars, 100 μm.

Figure S7. Blood vessel morphology and proliferation is defective in LC-depleted mice. Related to Figure 6.

(A) Maximum intensity projections of confocal imaging of CD31+ blood vessels (white) in whole mounts of naive skin from *huLang*-DTA mice. Scale bars, 500μm.

(B) Thickness (μm) of the leading edge of the angiogenic front in 5-day wounds from *huLang*-DTA and control mice. Error bars indicate mean +/- SEM. Data are 3-4 mice. unpaired T-test, ns, no statistical significance.

(C-D) Quantification of EdU+ fibroblasts (A) and immune cells (B) in 5-day wounds from *huLang*-DTA+ mice and DTA- littermate controls. Data are 4-5 mice. Error bars indicate mean +/- SEM. unpaired T-test, ns, no statistical significance.

Supplemental Table 1: Differential expression of mRNAs in endothelial cells in skin wounds. Endothelial cell genes differentially expressed (log2FC > 0.25 and adjusted p-value < 0.05) in ECs after wounding as compared to non-wounded conditions in scRNA-seq data[1](GSE142471).

Gene	*Avg log2FC*	*p_val adj*
Cst3	-2.23317011	9.06E-09
Scarb1	-1.845246649	1.21E-08
Lrat	-1.065294618	1.81E-08
Pltp	-1.798236885	4.03E-08
Bcam	-1.5112441	5.21E-07
S100a11	1.726695182	1.54E-06
Ly6c1	-1.735973687	1.31E-05
Apoe	-1.849026367	1.34E-05
Rasa4	-1.727694619	1.49E-05
Pfn1	1.522085415	3.34E-05
Slc30a1	-1.261881921	5.43E-05
Lgals1	1.961494528	7.61E-05
Cxcl2	1.700152683	9.04E-05
Cxx1a	-1.379714389	0.000278036
Marcksl1	1.888293587	0.000286667
Serf2	0.919003448	0.000364137
Thy1	-1.943512597	0.000376994
C1qtnf9	-1.166789174	0.000501279
Gm694	-1.393243848	0.000873614
Col18a1	1.658017547	0.000933449
Cxcl12	-0.91371648	0.001184977
Ndrg1	-1.301121202	0.001280278
Gng5	0.940905031	0.001540827
Lgals7	-1.352577217	0.001729223
Pecam1	-0.793078579	0.002085169
Grem1	-0.320095338	0.002519088
Fkbp1a	0.916923769	0.002686589
Krt5	-0.915270432	0.003920625
Fam167b	1.685649536	0.004175654
Rhoc	1.314569057	0.004298097
Col4a1	1.553729837	0.004467181
Fos	-1.839098959	0.005984115
Tmsb4x	0.742468256	0.006105735
Myct1	1.193931581	0.006159919
Prelid1	1.255318106	0.009846021
Rasd1	-1.765351526	0.011465308
Col4a2	1.341593648	0.015441265
Ctla2a	1.647316685	0.016993252
mt-Nd5	-1.311311095	0.018181983
Csrp2	1.306384981	0.022002879
Hspb1	-1.174456749	0.022692051
Cfl1	0.953394277	0.02445221
RP23-354H24.9	-0.381868488	0.030318575
Sectm1a	-0.807647815	0.03374519
Tgfbi	1.411284654	0.034643424

Slc3a2	-0.967478137	0.035642287
Myeov2	1.013767144	0.038626676
Bsg	-1.294635198	0.04121822
Sectm1b	-0.865868782	0.041749752
Hist1h2bc	1.725364748	0.046419627

Supplemental Table 2: References of mRNAs expressed by LCs that are predicted by NicheNet to control angiogenesis

LC expressed ligand/Cell surface protein predicted to control angiogenesis in skin wounds	Angiogenesis role	Reference
Cxcl16	Promotes endothelial cell proliferation, chemotaxis, and tube formation	[2,3]
Cd24a	Abrogates vascular remodeling and angiogenesis in retinopathy of prematurity (ROP) in a mouse model of oxygen-induced retinopathy	[4]
Flrt3	Promotes endothelial cell proliferation, chemotaxis, and tube formation	[5]
Pvr	Encodes Necl-5/poliovirus receptor. Regulates VEGF-induced angiogenesis by controlling the interaction of VEGFR2 with integrin α(v)β(3)	[6]
Efna1	Promotes tumor angiogenesis and neoangiogenesis	[7]
Sema7a	Promotes VEGF-mediated endothelial cell migration and proliferation in vitro; required for neovascularization in murine atherosclerotic plaques	[7,8]
Mmp9	Activates angiogenesis in vitro and in melanoma	[9]
Vegfa	Major regulator of vascular endothelial cell proliferation, migration and angiogenesis in vivo in multiple contexts	[10-14]
Pgf	Stimulates proliferation of endothelial cells in vitro	[15,16]
Ocln	Regulates VEGF retinal neovascularization; promotes tumour angiogenesis in bladder cancer cells and murine xenografts; facilitates VEGF signaling in retinal neovascularization	[17,18]
Itgb2	Component of CD11b, which supports VEGF secretion, supports Plm-dependent recruitment of myeloid cells to angiogenic niches and facilitates myeloid cell binding to endothelial cells during inflammation	[19]

Supplemental References

1. Haensel, D., Jin, S., Sun, P., Cinco, R., Dragan, M., Nguyen, Q., Cang, Z., Gong, Y., Vu, R., MacLean, A.L., et al. (2020). Defining Epidermal Basal Cell States during Skin Homeostasis and Wound Healing Using Single-Cell Transcriptomics. Cell Rep *30*, 3932-3947.e3936. 10.1016/j.celrep.2020.02.091.
2. Yu, X., Zhao, R., Lin, S., Bai, X., Zhang, L., Yuan, S., and Sun, L. (2016). CXCL16 induces angiogenesis in autocrine signaling pathway involving hypoxia-inducible factor 1α in human umbilical vein endothelial cells. Oncol Rep *35*, 1557-1565. 10.3892/or.2015.4520.
3. Zhuge, X., Murayama, T., Arai, H., Yamauchi, R., Tanaka, M., Shimaoka, T., Yonehara, S., Kume, N., Yokode, M., and Kita, T. (2005). CXCL16 is a novel angiogenic factor for human umbilical vein endothelial cells. Biochem Biophys Res Commun *331*, 1295-1300. 10.1016/j.bbrc.2005.03.200.
4. Newman, H., Shapira, S., Spierer, O., Kraus, S., Rosner, M., Pri-Chen, S., Loewenstein, A., Arber, N., and Barak, A. (2012). Involvement of CD24 in angiogenesis in a mouse model of oxygen-induced retinopathy. Curr Eye Res *37*, 532-539. 10.3109/02713683.2011.647226.
5. Jauhiainen, S., Laakkonen, J.P., Ketola, K., Toivanen, P.I., Nieminen, T., Ninchoji, T., Levonen, A.L., Kaikkonen, M.U., and Ylä-Herttuala, S. (2019). Axon Guidance-Related Factor FLRT3 Regulates VEGF-Signaling and Endothelial Cell Function. Front Physiol *10*, 224. 10.3389/fphys.2019.00224.
6. Kinugasa, M., Amano, H., Satomi-Kobayashi, S., Nakayama, K., Miyata, M., Kubo, Y., Nagamatsu, Y., Kurogane, Y., Kureha, F., Yamana, S., et al. (2012). Necl-5/poliovirus receptor interacts with VEGFR2 and regulates VEGF-induced angiogenesis. Circ Res *110*, 716-726. 10.1161/CIRCRESAHA.111.256834.
7. Beauchamp, A., and Debinski, W. (2012). Ephs and ephrins in cancer: ephrin-A1 signalling. Semin Cell Dev Biol *23*, 109-115. 10.1016/j.semcdb.2011.10.019.
8. Hu, S., Liu, Y., You, T., and Zhu, L. (2018). Semaphorin 7A Promotes VEGFA/VEGFR2-Mediated Angiogenesis and Intraplaque Neovascularization in. Front Physiol *9*, 1718. 10.3389/fphys.2018.01718.
9. Li, L., Fan, P., Chou, H., Li, J., Wang, K., and Li, H. (2019). Herbacetin suppressed MMP9 mediated angiogenesis of malignant melanoma through blocking EGFR-ERK/AKT signaling pathway. Biochimie *162*, 198-207. 10.1016/j.biochi.2019.05.003.
10. Cao, Y. (2014). VEGF-targeted cancer therapeutics-paradoxical effects in endocrine organs. Nat Rev Endocrinol *10*, 530-539. 10.1038/nrendo.2014.114.
11. Ferrara, N. (2002). VEGF and the quest for tumour angiogenesis factors. Nat Rev Cancer *2*, 795-803. 10.1038/nrc909.
12. Giacca, M., and Zacchigna, S. (2012). VEGF gene therapy: therapeutic angiogenesis in the clinic and beyond. Gene Ther *19*, 622-629. 10.1038/gt.2012.17.
13. Johnson, K.E., and Wilgus, T.A. (2014). Vascular Endothelial Growth Factor and Angiogenesis in the Regulation of Cutaneous Wound Repair. Adv Wound Care (New Rochelle) *3*, 647-661. 10.1089/wound.2013.0517.
14. Waldner, M.J., Wirtz, S., Jefremow, A., Warntjen, M., Neufert, C., Atreya, R., Becker, C., Weigmann, B., Vieth, M., Rose-John, S., and Neurath, M.F. (2010). VEGF receptor signaling links inflammation and tumorigenesis in colitis-associated cancer. J Exp Med *207*, 2855-2868. 10.1084/jem.20100438.

15. Cao, Y., Chen, H., Zhou, L., Chiang, M.K., Anand-Apte, B., Weatherbee, J.A., Wang, Y., Fang, F., Flanagan, J.G., and Tsang, M.L. (1996). Heterodimers of placenta growth factor/vascular endothelial growth factor. Endothelial activity, tumor cell expression, and high affinity binding to Flk-1/KDR. J Biol Chem *271*, 3154-3162. 10.1074/jbc.271.6.3154.
16. Dull, R.O., Yuan, J., Chang, Y.S., Tarbell, J., Jain, R.K., and Munn, L.L. (2001). Kinetics of placenta growth factor/vascular endothelial growth factor synergy in endothelial hydraulic conductivity and proliferation. Microvasc Res *61*, 203-210. 10.1006/mvre.2000.2298.
17. Yang, F., Liu, X.Q., He, J.Z., Xian, S.P., Yang, P.F., Mai, Z.Y., Li, M., Liu, Y., and Zhang, X.D. (2022). Occludin facilitates tumour angiogenesis in bladder cancer by regulating IL8/STAT3 through STAT4. J Cell Mol Med *26*, 2363-2376. 10.1111/jcmm.17257.
18. Liu, X., Dreffs, A., Díaz-Coránguez, M., Runkle, E.A., Gardner, T.W., Chiodo, V.A., Hauswirth, W.W., and Antonetti, D.A. (2016). Occludin S490 Phosphorylation Regulates Vascular Endothelial Growth Factor-Induced Retinal Neovascularization. Am J Pathol *186*, 2486-2499. 10.1016/j.ajpath.2016.04.018.
19. Soloviev, D.A., Hazen, S.L., Szpak, D., Bledzka, K.M., Ballantyne, C.M., Plow, E.F., and Pluskota, E. (2014). Dual role of the leukocyte integrin αMβ2 in angiogenesis. J Immunol *193*, 4712-4721. 10.4049/jimmunol.1400202.